



A new multiscale air pollutant transport model using anisotropic adaptive mesh methods

J. Zheng et al.

A new multiscale air quality transport model (Fluidity, 4.1.9) using fully unstructured anisotropic adaptive mesh technology

J. Zheng^{1,2,4}, J. Zhu², Z. Wang¹, F. Fang³, C. C. Pain³, and J. Xiang³

¹State Key Laboratory of Atmospheric Boundary Layer Physics and Atmospheric Chemistry, Institute of Atmospheric Physics, Chinese Academy of Sciences, Beijing 100029, China

²International Center for Climate and Environment Sciences, Institute of Atmospheric Physics, Chinese Academy of Sciences, Beijing 100029, China

³Applied Modelling and Computation Group, Department of Earth Science and Engineering, Imperial College London, Prince Consort Road, London, SW7 2BP, UK

⁴University of Chinese Academy of Sciences, Beijing 100049, China

Received: 26 March 2015 – Accepted: 7 May 2015 – Published: 5 June 2015

Correspondence to: F. Fang (f.fang@imperial.ac.uk)

Published by Copernicus Publications on behalf of the European Geosciences Union.

Title Page

Abstract

Introduction

Conclusions

References

Tables

Figures



Back

Close

Full Screen / Esc

Printer-friendly Version

Interactive Discussion



Abstract

A new anisotropic hr-adaptive mesh technique has been applied to modelling of multiscale transport phenomena, which is based on a discontinuous Galerkin/control volume discretization on unstructured meshes. Over existing air quality models typically based on static-structured grids using a locally nesting technique, the advantage of the anisotropic hr-adaptive model has the ability to adapt the mesh according to the evolving pollutant distribution and flow features. That is, the mesh resolution can be adjusted dynamically to simulate the pollutant transport process accurately and effectively. To illustrate the capability of the anisotropic adaptive unstructured mesh model, three benchmark numerical experiments have been setup for two-dimensional (2-D) transport phenomena. Comparisons have been made between the results obtained using uniform resolution meshes and anisotropic adaptive resolution meshes.

1 Introduction

It is well known that the interaction of multiscale physical processes in atmospheric phenomena poses a formidable challenge for numerical modelling (Kühnlein, 2011). Large scale processes can trigger small scale features that again have an important influence/feed-back to the large scale (Behrens, 2007). For example, the processes of tropical cyclone involve a range over a continuous spectrum of scales from the large-scale flow environment $\sim \mathcal{O}(10^6-10^7)$ m, tropical cyclone itself $\sim \mathcal{O}(10^5-10^6)$ m, embedded eyewall and rainbands $\sim \mathcal{O}(10^3-10^4)$ m, down to microscales of the boundary layer turbulence $\sim \mathcal{O}(10-10^2)$ m (Kühnlein, 2011). Due to the highly disparate scales involved, global mesh refinement is not a viable option. Thus mesh adaptation may be the only effective way to resolve these multiscale geophysical flows accurately (Kühnlein, 2011; Weller et al., 2010; Nikiforakis, 2009).

So far, the accurate numerical modelling of advection (or transport) remains a central problem for many applications such as air pollution, atmospheric chemistry, meteorol-

GMDD

8, 4337–4374, 2015

A new multiscale air pollutant transport model using anisotropic adaptive mesh methods

J. Zheng et al.

Title Page

Abstract

Introduction

Conclusions

References

Tables

Figures

◀

▶

◀

▶

Back

Close

Full Screen / Esc

Printer-friendly Version

Interactive Discussion

A new multiscale air pollutant transport model using anisotropic adaptive mesh methods

J. Zheng et al.

[Title Page](#)

[Abstract](#)

[Introduction](#)

[Conclusions](#)

[References](#)

[Tables](#)

[Figures](#)

[⏪](#)

[⏩](#)

[◀](#)

[▶](#)

[Back](#)

[Close](#)

[Full Screen / Esc](#)

[Printer-friendly Version](#)

[Interactive Discussion](#)

ogy and other physical sciences. There have been many studies on the numerical advection schemes (e.g. PPM, Bott and Walcek etc.) which have been used in many air quality models (e.g. CMAQ, CMAx, NAQPMS etc.) (Colella and Woodward, 1984; Bott, 1989; Walcek and Aleksic, 1998). These advection algorithms were implemented based on a fixed uniform mesh system. The successive global refinement can be used to capture the details of small scale flow features, but is prohibitively expensive and not feasible for practical applications. Alternatively, the nesting technique, placing finer meshes within coarser meshes, is often used for achieving local higher resolution in many air quality models (Garcia-Menendez and Odman, 2011; Frohn et al., 2002; Wang, 2001). In static mesh nesting, the solutions obtained from the global coarse mesh model provide the boundary conditions for the nested mesh regional model, in turn, the solutions in the global model are updated with the high resolution solutions. However this may lead to spurious oscillations at the interface between the coarse mesh and nested fine mesh, especially when concentration gradients is large cross the interface. Although the numeral techniques such as blending, nudging, and selective damping approaches can be used to remove these oscillations, the small scale features on the fine meshes may be damped (Garcia-Menendez and Odman, 2011; Zhang et al., 1986; Debreu and Blayo, 2008; Alapaty et al., 1998). Moreover, due to highly unsteady atmospheric flows, it is almost impossible to construct a static optimal nested mesh suitable for an accuracy simulation over a long time period. The use of dynamically adaptive mesh techniques can therefore be considered so that the mesh resolution can be adjusted locally in response to the evolution of the flow and passive tracer (Piggott et al., 2009; Behrens, 2007).

In contrast to locally nested mesh techniques, adaptive mesh techniques not only can resolve multiscale processes in a consistent way, but also can enable to follow and capture the features of flows as time evolves. Dynamic mesh adaptation can be achieved, either by relocating mesh nodes or by locally increasing (and decreasing) the number of nodes in time and space. The former, known as mesh movement (i.e. r-adaptivity), can be used to improve the accuracy of solutions by optimally re-

A new multiscale air pollutant transport model using anisotropic adaptive mesh methods

J. Zheng et al.

[Title Page](#)

[Abstract](#)

[Introduction](#)

[Conclusions](#)

[References](#)

[Tables](#)

[Figures](#)

[⏪](#)

[⏩](#)

[◀](#)

[▶](#)

[Back](#)

[Close](#)

[Full Screen / Esc](#)

[Printer-friendly Version](#)

[Interactive Discussion](#)



locating mesh nodes to resolve the small scale features of interest (Garcia-Menendez and Odman, 2011; Srivastava et al., 2000; Lagzi et al., 2009; Kühnlein et al., 2012; Nikiforakis, 2009). However, the accuracy of solutions using r-adaptivity is restricted by a priori for achieving an optimal dynamic mesh (where the total number of nodes is fixed). The latter, known as mesh enrichment (i.e. h-adaptivity), can guarantee a minimum solution accuracy level by providing sufficient resolution where and when it is needed (Baker et al., 2013; Constantinescu et al., 2008; Piggott et al., 2005). Various h-adaptive techniques based on structured meshes as well as the r-adaptive techniques on unstructured/structured meshes have been explored in atmospheric modeling. And some of these techniques have been applied to air quality models (Garcia-Menendez and Odman, 2011). Recently, significant research efforts have been focused on application of this new adaptive mesh techniques in ocean modeling (Pain et al., 2005; Piggott et al., 2009, 2008a, b).

This article applies a new anisotropic hr-adaptive mesh technique into two-dimensional (2-D) air quality transport modelling. This adaptive unstructured mesh technique provides the dynamic spatial and temporal resolution to capture moving features, e.g. moving fronts or dust storm. Using the hr-adaptive technique, existing elements can be split (h-adaptive) or element vertices can be moved (r-adaptive), to periodically modify the mesh geometry. Hence, the purpose of this article is to demonstrate, through example problems, the capability of anisotropic mesh adaptivity for modelling of multiscale transport phenomena.

The remaining structure of this article is as follows: Sect. 2 describes numerical advection methods, including discontinuous Galerkin (DG) and control volume (CV) methods based on unstructured meshes. Section 3 covers the topics of mesh adaptivity, error measures and interpolation. Section 4 introduces 3-D unstructured anisotropic adaptive mesh model (Fluidity). In Sect. 5, results in three benchmark tests are presented and discussed for a two-dimensional scalar advection problem. Conclusions are drawn in Sect. 6.

A new multiscale air pollutant transport model using anisotropic adaptive mesh methods

J. Zheng et al.

Title Page

Abstract

Introduction

Conclusions

References

Tables

Figures

◀

▶

◀

▶

Back

Close

Full Screen / Esc

Printer-friendly Version

Interactive Discussion



where, the hatted term represents fluxes across the element facets. Due to the discontinuous nature of fields, there is no unique value for the flux term, however the requirement that c is a conserved quantity, does demand that adjacent elements make a consistent choice for the flux between them. In this work, two advective flux schemes, the upwind and local Lax-Friedrichs flux methods, are used to represent $\widehat{\mathbf{n} \cdot \mathbf{u} c}$ for DG methods (AMCG, 2014). In $\widehat{\mathbf{n} \cdot \mathbf{u} c}$, the advecting velocity \mathbf{u} can be calculated by either averaging it on each side of the face or applying a Galerkin projection to project the velocity onto a continuous basis.

In the upwind flux formulation, the value of c at each quadrature point on the face is taken to be the upwind value, that is, if fluid is into/out of the element then it is the value on the exterior/interior side of the face. Integrating the advection term by part twice, then Eq. (3) becomes (AMCG, 2014):

$$\sum_e \left\{ \int_e \left(\phi \frac{\partial c}{\partial t} - \phi \hat{\mathbf{u}} \cdot \nabla c \right) de + \int_{\partial e \cap \partial \Omega} \mathbf{n} \cdot \hat{\mathbf{u}} (c_b - c_{\text{int}}) d\partial e + \int_{\partial e \setminus \partial \Omega} \mathbf{n} \cdot \hat{\mathbf{u}} (c_{\text{ext}} - c_{\text{int}}) d\partial e \right\} = 0, \quad (4)$$

where, $\hat{\mathbf{u}}$ represents the flux velocity and a weakly imposed boundary condition $c = c_b$ is applied on the inflow part of boundaries; c_{ext} and c_{int} are the values on the exterior and interior side of the face respectively.

In local Lax–Friedrichs flux formulation, the tracer advection is given by:

$$\widehat{\mathbf{n} \cdot \mathbf{u} c} = \frac{1}{2} \mathbf{n} \cdot \hat{\mathbf{u}} (c_{\text{int}} + c_{\text{ext}}) - \frac{C}{2} (c_{\text{int}} - c_{\text{ext}}), \quad (5)$$

where for each facet $s \subset \partial e$:

$$C = \sup_{x \in s} |\hat{\mathbf{u}} \cdot \mathbf{n}|. \quad (6)$$

To ensure nonlinear stability and effectively suppress spurious oscillations, the slope limiting techniques are used here (Kuzmin, 2010; Cockburn and Shu, 2001; Luo et al., 2007).

2.1.2 Control volume discretization

The control volume discretization uses a dual mesh constructed around the nodes of the parent finite element mesh. Once the dual control volume mesh has been defined, it is possible to discretise the advection Eq. (1) using piecewise constant shape functions within each volume, v . Integrating Eq. (1) by parts within a volume, v and summing over all volumes, we obtain:

$$\sum_v \left\{ \int_v \frac{\partial c}{\partial t} + \sum_k \int_{\partial v_k} \widehat{\mathbf{n} \cdot \mathbf{u}} c_k \right\} = 0, \quad (7)$$

here, the velocity is well-defined since the control volume facets are in the center of the elements of the parent mesh where it is continuous. The value of c_k is computed at each quadrature point of the facet k using the finite element interpolation approach, i.e. interpolating it using the finite element basis functions on the parent mesh. Usually the first order quadrature is performed on the control volume facets, however if higher order control volume facet quadrature is selected then k refers to each quadrature point on the facet. To avoid the spurious oscillations, the Sweby flux limiter is used to make the solutions total variation diminishing (Sweby, 1984; Leonard, 1991; Waterson and Deconinck, 2007; Wilson, 2009; LeVeque, 2002).

2.2 Time discretization

The semi-discrete matrix form of Eq. (2) can be written as

$$\mathbf{M} \frac{dc}{dt} + \mathbf{A}(\mathbf{u})c = r, \quad (8)$$

A new multiscale air pollutant transport model using anisotropic adaptive mesh methods

J. Zheng et al.

[Title Page](#)

[Abstract](#)

[Introduction](#)

[Conclusions](#)

[References](#)

[Tables](#)

[Figures](#)

[⏪](#)

[⏩](#)

[◀](#)

[▶](#)

[Back](#)

[Close](#)

[Full Screen / Esc](#)

[Printer-friendly Version](#)

[Interactive Discussion](#)



in which the vector $\mathbf{c} = (c_1, \dots, c_{\mathcal{N}})^T$ contains the solution of variable c at nodes (\mathcal{N} is the number of nodes); \mathbf{r} is the right-hand side vector containing boundary, source and absorption terms; \mathbf{M} is the mass matrix; and $\mathbf{A}(\mathbf{u})$ is the advection operator, where for continuous Galerkin:

$$\mathbf{M}_{ij} = \int_{\Omega} \phi_i \phi_j, \quad \mathbf{A}_{ij} = - \int_{\Omega} \nabla \phi_i \cdot \mathbf{u} \phi_j, \quad i, j \in (1, 2, \dots, \mathcal{N}). \quad (9)$$

The time derivative term at time level $n + 1$ is treated using the θ -method to yield

$$\mathbf{M} \frac{\mathbf{c}^{n+1} - \mathbf{c}^n}{\Delta t} + \mathbf{A}(\mathbf{u}^{n+\theta}) \mathbf{c}^{n+\theta} = \mathbf{r}^{n+\theta}. \quad (10)$$

where $\theta \in [0, 1]$ and the terms $\mathbf{c}^{n+\theta}$ are given by,

$$\mathbf{c}^{n+\theta} = \theta \mathbf{c}^{n+1} + (1 - \theta) \mathbf{c}^n. \quad (11)$$

Equation (10) can be rearranged for unknown vector \mathbf{c}^{n+1} :

$$\left(\mathbf{M} + \theta \Delta t \left(\mathbf{A} \left(\mathbf{u}^{n+\theta} \right) \right) \right) \mathbf{c}^{n+1} = \left(\mathbf{M} - (1 - \theta) \Delta t \left(\mathbf{A} \left(\mathbf{u}^{n+\theta} \right) \right) \right) \mathbf{c}^n + \mathbf{r}^{n+\theta}. \quad (12)$$

3 Mesh adaptivity

The optimization-based adaptivity technique developed by the Applied Modelling and Computation Group (AMCG) at Imperial College London (AMCG, 2014), is introduced in this section. It utilizes dynamic adaptation of a fully unstructured triangular (or tetrahedral) mesh in two (or three)-dimensions, as presented in (Pain et al., 2001, 2005; Piggott et al., 2009). The unstructured and adaptive meshes allow computational effort to resolve important fluid dynamics at diverse scales. The key objective of using

GMDD

8, 4337–4374, 2015

A new multiscale air pollutant transport model using anisotropic adaptive mesh methods

J. Zheng et al.

Title Page

Abstract

Introduction

Conclusions

References

Tables

Figures

◀

▶

◀

▶

Back

Close

Full Screen / Esc

Printer-friendly Version

Interactive Discussion



A new multiscale air pollutant transport model using anisotropic adaptive mesh methods

J. Zheng et al.

Title Page

Abstract

Introduction

Conclusions

References

Tables

Figures

◀

▶

◀

▶

Back

Close

Full Screen / Esc

Printer-friendly Version

Interactive Discussion

mesh adaptivity. However, the consistent interpolation can introduce a suboptimal interpolation error, unsuitability for discontinuous fields, and lack of conservation. An alternative conservative interpolation approach, the Galerkin projection is proposed for discontinuous fields. A supermeshing algorithm (Farrell et al., 2009) is used for implementation of the Galerkin projection.

4 Introduction of a 3-D unstructured anisotropic adaptive mesh model (Fluidity, 4.1.9)

The new multiscale air quality transport model has been developed with a 3-D unstructured and adaptive mesh model (Fluidity, developed by the Applied Modelling and Computation Group (AMCG) at Imperial College London). Fluidity, an open source LGPL model, is a general purpose multiphase CFD code which is capable of modelling a wide range of fluid phenomena involving single and multiphase flows. It numerically solves the 2-D/3-D Navier–Stokes equation (being non-hydrostatic, to model dense water formation and flows over steep topography) and field equations with a range of control volume and finite element discretisation methods. Its modelling framework has been developed through the cross-fertilisation of techniques and experiences in engineering fluids, oceanography, atmospheric dynamics, air pollution, impact cratering, inversion, radiation transport, coupled multi-physics modelling, multi-phase flows and fluid-structure interactions. This has led to a number of novel, advanced methods based upon adapting and moving anisotropic unstructured meshes, advanced finite element and control volume discretisations, and a range of numerical stabilisation and Large Eddy Simulation (LES) turbulence models. Among existing unstructured mesh models, Fluidity is the only model that can simultaneously resolve both small- and large-scale fluid flows while smoothly varying resolution and conforming to complex topography. The model employs 3-D anisotropic mesh adaptivity to resolve and reveal fine scale features as they develop while reducing resolution elsewhere. A number of

interpolation methods (e.g., non conservative point-wise and conservative methods) are available for mesh-to-mesh interpolations between adaptations.

Fluidity is parallelised using MPI and is capable of scaling to many thousands of processors. It has a user-friendly GUI and a python interface which can be used to calculate diagnostic fields, set prescribed fields or set user-defined boundary conditions (for details, see <https://www.imperial.ac.uk/engineering/departments/earth-science/research/research-groups/amcg/>).

5 Numerical examples

To illustrate the efficiency and accuracy of anisotropic adaptive schemes, three benchmark problems have been adopted which are representative and challenging enough to predict how the new adaptive multiscale model would behave in future real-life applications (LeVeque, 1996; Kuzmin, 2009; Staniforth et al., 1987; Walcek and Aleksic, 1998; Bott, 1989, 1993, 2010).

In the following comparative study, we consider FEM_Fix and FEM_Adapt schemes (FEM represents CV or DG) based on the control volume and discontinuous Galerkin discretization in the same computational domain $\Omega = [0, 1] \times [0, 1]$. The CV_Fix_L and DG_Fix_L schemes use fixed uniform triangular meshes while the CV_Adapt_L and DG_Adapt_L schemes use adaptive meshes (where L represents the different mesh schemes, as shown in Table 1). For CV discretization, a finite element interpolation is used at the control volume faces in combination with a Sweby slope limiter to bound the solution. The time discretization used here is the classical Crank–Nicolson scheme ($\theta = 0.5$). For DG discretization, the upwind flux is chosen in combination with vertex-based slope limiter. The slope limiter used with the discontinuous Galerkin formulation only guarantee a bounded solution in conjunction with an explicit advection scheme. Therefore, advection subcycling based upon a CFL criterion is necessary for DG discretization (AMCG, 2014).

A new multiscale air pollutant transport model using anisotropic adaptive mesh methods

J. Zheng et al.

Title Page

Abstract

Introduction

Conclusions

References

Tables

Figures

◀

▶

◀

▶

Back

Close

Full Screen / Esc

Printer-friendly Version

Interactive Discussion



Equation (12) is solved by the generalized minimum residual method (Saad, 1993). The successive over-relaxation preconditioned is invoked to speed up convergence at large time steps.

To assess the difference between the analytical solution c and its numerical approximation c_h , we introduce the error norms:

$$E_1 = \int_{\Omega} |c - c_h| d\Omega = \|c - c_h\|_1, \quad (16)$$

$$E_2 = \sqrt{\int_{\Omega} |c - c_h|^2 d\Omega} = \|c - c_h\|_2. \quad (17)$$

5.1 Case one: solid body revolution

A standard test problem applied to the convection equation (1) in 2-D is solid body revolution (LeVeque, 1996; Kuzmin, 2009). The incompressible velocity field in the domain $\Omega = [0, 1] \times [0, 1]$ is represented by

$$\mathbf{u}(x, y) = (0.5 - y, x - 0.5), \quad (18)$$

which corresponds to a counterclockwise rotation around the center (0.5,0.5) of Ω . Following LeVeque (1996), we consider a slotted cylinder, a sharp cone, and a smooth hump as the initial solid bodies defined within the circle centered at each reference point (x_0, y_0) :

$$r(x, y) = \frac{1}{r_0} \sqrt{(x - x_0)^2 + (y - y_0)^2} \leq 1, \quad (19)$$

where $r_0 = 0.15$. After each full revolution ($t = 2\pi k$), the exact solution return to the initial distribution as depicted in Fig. 1. For the slotted cylinder, the reference point is

mesh schemes. Hence, the use of adaptive meshes provides an efficient approach to lower the storage requirement, thus leading to the reduction of the overall computing time while remaining the accuracy of numerical results.

Figure 4 shows the numerical results at $t = 2\pi$ (after one full revolution) using the adaptive and fixed mesh schemes. For comparison purpose, the FEM_Fix_1 and FEM_Adapt_4 schemes are chosen since the number of nodes in these two mesh schemes are almost same, where $N = 10\,201$ for FEM_Fix_1 scheme while $N \approx 11\,500$ for FEM_Adapt_4 scheme. The solutions of CV_Fix_1 and DG_Fix_1 are computed on a structured uniform mesh of triangular elements with mesh size $h = 1/100$ and $\Delta t = 0.01$. It can be seen that there is severe erosion of the slotted cylinder when the fixed mesh scheme is adopted. The adaptive mesh scheme provides an improvement in accuracy of results. It is shown that with use of adaptive meshes (especially DG Adapt_Adapt_4), the initial shape of bodies is preserved well.

5.2 Case two: swirling flow

The capability of the adaptive mesh model has been further demonstrated in modelling swirling flow phenomena. The set up of the simulation in this case is similar with case one, however the velocity field is provided by the formula (LeVeque, 1996; Kuzmin, 2009):

$$\mathbf{u}(x, y, t) = (\sin^2(\pi x) \sin(2\pi y)g(t), -\sin^2(\pi y) \sin(2\pi x)g(t)) \quad (23)$$

where $g(t) = \cos(\pi t/T)$ on the time interval $0 \leq t \leq T$ (here $T = 1$).

The initial mass distribution will be deformed by the time-dependent velocity field which gradually slows down to zero and reverses its direction at $t = T/2$. Thus, the initial profile will be reproduced at the final time $t = T$ as depicted in Fig. 1.

A comparison of results using fixed and adaptive meshes is illustrated in Figs. 5–8. Again, it can be observed that by using the adaptive mesh scheme in the model, both the CPU time and number of nodes required are significantly reduced for a given level of accuracy of results (see Fig. 6). To improve the stability of solutions when the mesh

A new multiscale air pollutant transport model using anisotropic adaptive mesh methods

J. Zheng et al.

Title Page

Abstract

Introduction

Conclusions

References

Tables

Figures

◀

▶

◀

▶

Back

Close

Full Screen / Esc

Printer-friendly Version

Interactive Discussion



where $A = 0.08$, $k = 4\pi$.

The results using anisotropic adaptive meshes have been compared with those using Walcek scheme presented in Walcek and Aleksic (1998). The analytical solutions were depicted in (Staniforth et al., 1987). Figures 11 and 12 show the comparison of three different schemes' results with the analytical solution at time $t = 3T/20$ and $t = T/5$, where $T = 2.6376$. The solutions of the Walcek scheme were computed on a structured uniform mesh with $h = 1/200$ and $\Delta t = 0.003297$. For FEM_Adapt_128 schemes (see Table 1), they were computed on dynamic adaptive mesh with constant $\Delta t = 0.006594$. The minimum mesh size is 7.8125×10^{-6} while the maximum mesh size is 0.2.

It can be observed the initial c field is split into two rotations within the areas of the two central vertices as time evolves. Since the spatial gradient of solutions increases as time evolves especially at the boundaries of the central vortices, high resolution of meshes around the boundaries is needed to present the sharp shape accurately. Due to lack of high resolution of meshes, the solutions using the Walcek scheme fail to represent the analytical one and maintain the shape distribution. For the Walcek scheme, at time $t = 3T/20$ (see Fig. 11), the gradients of numerical distribution begin to disappear at the upper and middle boundaries of the central vortices and nearly completely disappear at time $t = T/5$ (Fig. 12). By adapting the mesh in time and space, the mesh resolution increases around the boundaries of each vertice, thus improving the accuracy of results. There is close agreement between the adaptive mesh modelling results and the analytical ones although the gradients for CV_Adapt_128 scheme are not as strong as the exact solution.

The sequence of triangulations presented in Fig. 13 demonstrates that the dynamic mesh adaptation algorithm succeeds in locally refining the mesh in the vicinity of steep fronts so as to reduce the amount of numerical diffusion and follow steep fronts as time evolves. To further reduce the number of elements, the anisotropic adaptive algorithm has been used for all the above adaptive mesh scheme, allowing the mesh is adapted along different directions. As shown in Fig. 14 which depicts a closeup view of locally adapted mesh, the adapted mesh size across the boundaries is small enough to cap-

GMDD

8, 4337–4374, 2015

A new multiscale air pollutant transport model using anisotropic adaptive mesh methods

J. Zheng et al.

Title Page

Abstract

Introduction

Conclusions

References

Tables

Figures

◀

▶

◀

▶

Back

Close

Full Screen / Esc

Printer-friendly Version

Interactive Discussion

ture the sharp fronts while large along the boundaries since the c field does not change much. Therefore, the mesh sizing desired in anisotropic adaptive algorithm is not only a function of space, it is also a function of direction. At a given point, the desired mesh sizing differs in different directions.

Figure 15 shows the number of nodes required for CV_Adapt_128 scheme is less than the node number (40 000) for fixed Walcek scheme during most of the simulation period. However, as local mesh resolution increases with time, the max CFL number of CV_Adapt_128 scheme exceeds unit. To keep the stabilization of solutions, the Crank–Nicolson scheme is adopted here. In this way, the use of a large time step is acceptable when applying adaptive mesh techniques into comprehensive air quality models, which can make the computation much more efficient. As shown in Fig. 15, in combination with the Crank–Nicolson method, the adaptive mesh CV modelling solutions can maintain stable and accurate without reducing the time step size even if the max CFL number of CV_Adapt_128 exceeds 80. All of these can further illustrate the efficiency and the potential of dynamic mesh adaptation for future real applications in air quality model.

6 Conclusions

In this paper, a new anisotropic adaptive mesh technique has been introduced and applied to modelling of multi-scale transport phenomena, which is a central component in air quality modelling systems. The first two benchmark test cases using the fixed mesh and adapted mesh schemes have been setup to illustrate the efficiency and accuracy of anisotropic adaptive mesh technique, which is an important means to improve the competitiveness of unstructured mesh air quality models. The last case presents the irreplaceable advantage of this new adaptive mesh method to reveal detailed small scale plume structure (large gradients) that cannot be resolved with static grids, using comparable computational resources.

A new multiscale air pollutant transport model using anisotropic adaptive mesh methods

J. Zheng et al.

Title Page

Abstract

Introduction

Conclusions

References

Tables

Figures

⏪

⏩

◀

▶

Back

Close

Full Screen / Esc

Printer-friendly Version

Interactive Discussion



A new multiscale air pollutant transport model using anisotropic adaptive mesh methods

J. Zheng et al.

Title Page

Abstract

Introduction

Conclusions

References

Tables

Figures

⏪

⏩

◀

▶

Back

Close

Full Screen / Esc

Printer-friendly Version

Interactive Discussion

It is demonstrated that the dynamic anisotropic adaptive mesh technique can be used to automatically adapt the mesh resolution to follow the evolving pollutant and transient flow features in time and space, thus reducing the CPU time and memory requirement significantly. In combination with the Crank–Nicolson method, the adaptive mesh air pollution model is able to maintain the stability and accuracy of results without reducing the time step size when the minimum mesh size is getting smaller. This is of great significance for the future applications in multiscale modeling.

The last test case serves as a proof-of-concept to further illustrate the capability of anisotropic mesh adaptivity techniques. In this case, the swirling deformation flow exhibits very high aspect ratios (1000, for example), which means that the pollutant distribution can possess very strong anisotropies as time evolves. Hence, the anisotropic mesh adaptation provides a very useful and effective way to simulate and represent this special atmospheric phenomena.

In summary, the results obtained in this work show the capability and potential of adaptive mesh methods to simulate multiscale air pollutant transport problems (spanning a range of scales) with higher numerical accuracy. The mesh adaptation can be used to improve the mesh resolution when and where it is needed without performing successive global refinement which is prohibitively expensive, and therefore, not feasible for realistic applications. Future work will consider emissions and meteorological data as inputs to further demonstrate the capability of dynamic adaptive mesh techniques.

Code availability

Fluidity code developed by the Applied Modelling and Computation Group (AMCG) at Imperial College London is available under the GNU General Public License (<https://github.com/FluidityProject/fluidity>). The user manual and examples are also available.

Acknowledgements. This work was carried out under funding from the Chinese Academy of Sciences (CAS) Strategic Priority Research Program (Grant No. XDB05030200), the UK's Natural Environment Research Council (projects NER/A/S/2003/00595, NE/C52101X/1 and

NE/C51829X/1), the Engineering and Physical Sciences Research Council (GR/R60898, EP/I00405X/1 and EP/J002011/1) and the Imperial College High Performance Computing Service. The authors would like to thanks to J. Percival for many helpful discussions and support from others in AMCG.

5 References

- Alapaty, K., Mathur, R., and Odman, T.: Intercomparison of spatial interpolation schemes for use in nested grid models, *Mon. Weather Rev.*, 126, 243–249, 1998. 4339
- AMCG: Fluidity Manual, Applied Modelling and Computation Group, Imperial College London, 2014. 4342, 4344, 4345, 4347
- 10 Baker, C., Buchan, A., Pain, C., Farrell, P., Eaton, M., and Warner, P.: Multimesh anisotropic adaptivity for the Boltzmann transport equation, *Ann. Nucl. Energy*, 53, 411–426, 2013. 4340
- Behrens, J.: Adaptive Atmospheric Modeling: Key Techniques in Grid Generation, Data Structures, and Numerical Operations with Applications, Springer Science & Business Media, Vol. 54, 1–22, 2007. 4338, 4339
- 15 Bott, A.: A positive definite advection scheme obtained by nonlinear renormalization of the advective fluxes, *Mon. Weather Rev.*, 117, 1006–1016, 1989. 4339, 4347
- Bott, A.: The monotone area-preserving flux-form advection algorithm: reducing the time-splitting error in two-dimensional flow fields, *Mon. Weather Rev.*, 121, 2637–2641, 1993. 4347
- 20 Bott, A.: Improving the time-splitting errors of one-dimensional advection schemes in multidimensional applications, *Atmos. Res.*, 97, 619–631, 2010. 4347, 4351
- Burbeau, A., Sagaut, P., and Bruneau, C.-H.: A problem-independent limiter for high-order Runge–Kutta discontinuous Galerkin methods, *J. Comput. Phys.*, 169, 111–150, 2001. 4341
- Cockburn, B. and Shu, C.-W.: Runge–Kutta discontinuous Galerkin methods for convection-dominated problems, *J. Sci. Comput.*, 16, 173–261, 2001. 4341, 4343
- 25 Cockburn, B., Karniadakis, G. E., and Shu, C.-W.: The Development of Discontinuous Galerkin Methods, Springer, 1–20, 2000. 4341
- Colella, P. and Woodward, P. R.: The piecewise parabolic method (PPM) for gas-dynamical simulations, *J. Comput. Phys.*, 54, 174–201, 1984. 4339

A new multiscale air pollutant transport model using anisotropic adaptive mesh methods

J. Zheng et al.

Title Page

Abstract

Introduction

Conclusions

References

Tables

Figures

◀

▶

◀

▶

Back

Close

Full Screen / Esc

Printer-friendly Version

Interactive Discussion



A new multiscale air pollutant transport model using anisotropic adaptive mesh methods

J. Zheng et al.

[Title Page](#)

[Abstract](#)

[Introduction](#)

[Conclusions](#)

[References](#)

[Tables](#)

[Figures](#)

[⏪](#)

[⏩](#)

[◀](#)

[▶](#)

[Back](#)

[Close](#)

[Full Screen / Esc](#)

[Printer-friendly Version](#)

[Interactive Discussion](#)



- Kuzmin, D.: A vertex-based hierarchical slope limiter for p-adaptive discontinuous Galerkin methods, *J. Comput. Appl. Math.*, 233, 3077–3085, 2010. 4343
- Lagzi, I., Turányi, T., Tomlin, A. S., and Haszpra, L.: Modelling photochemical air pollutant formation in Hungary using an adaptive grid technique, *Int. J. Environ. Pollut.*, 36, 44–58, 2009. 4340
- Leonard, B.: The ULTIMATE conservative difference scheme applied to unsteady one-dimensional advection, *Comput. Method. Appl. M.*, 88, 17–74, 1991. 4343
- LeVeque, R. J.: High-resolution conservative algorithms for advection in incompressible flow, *SIAM J. Numer. Anal.*, 33, 627–665, 1996. 4347, 4348, 4350
- LeVeque, R. J.: *Finite Volume Methods for Hyperbolic Problems*, Vol. 31, Cambridge University Press, 2002. 4343
- Luo, H., Baum, J. D., and Löhner, R.: A Hermite WENO-based limiter for discontinuous Galerkin method on unstructured grids, *J. Comput. Phys.*, 225, 686–713, 2007. 4343
- Nikiforakis, N.: Mesh generation and mesh adaptation for large-scale Earth-system modelling, *Philos. T. R. Soc. A*, 367, 4473–4481, 2009. 4338, 4340
- Pain, C., Umpelby, A., De Oliveira, C., and Goddard, A.: Tetrahedral mesh optimisation and adaptivity for steady-state and transient finite element calculations, *Comput. Method. Appl. M.*, 190, 3771–3796, 2001. 4344
- Pain, C., Piggott, M., Goddard, A., Fang, F., Gorman, G., Marshall, D., Eaton, M., Power, P., and De Oliveira, C.: Three-dimensional unstructured mesh ocean modelling, *Ocean Model.*, 10, 5–33, 2005. 4340, 4344
- Piggott, M., Pain, C., Gorman, G., Power, P., and Goddard, A.: h, r, and hr adaptivity with applications in numerical ocean modelling, *Ocean Model.*, 10, 95–113, 2005. 4340
- Piggott, M., Gorman, G., Pain, C., Allison, P., Candy, A., Martin, B., and Wells, M.: A new computational framework for multi-scale ocean modelling based on adapting unstructured meshes, *Int. J. Numer. Meth. Fl.*, 56, 1003–1015, 2008a. 4340
- Piggott, M. D., Pain, C. C., Gorman, G. J., Marshall, D. P., and Killworth, P. D.: Unstructured adaptive meshes for ocean modeling, *Geoph. Monog. Series*, 177, 383–408, 2008b. 4340
- Piggott, M., Farrell, P., Wilson, C., Gorman, G., and Pain, C.: Anisotropic mesh adaptivity for multi-scale ocean modelling, *Philos. T. R. Soc. A*, 367, 4591–4611, 2009. 4339, 4340, 4344
- Saad, Y.: A flexible inner-outer preconditioned GMRES algorithm, *SIAM J. Sci. Comput.*, 14, 461–469, 1993. 4348

GMDD

8, 4337–4374, 2015

**A new multiscale air
pollutant transport
model using
anisotropic adaptive
mesh methods**

J. Zheng et al.

[Title Page](#)
[Abstract](#)
[Introduction](#)
[Conclusions](#)
[References](#)
[Tables](#)
[Figures](#)
[⏪](#)
[⏩](#)
[◀](#)
[▶](#)
[Back](#)
[Close](#)
[Full Screen / Esc](#)
[Printer-friendly Version](#)
[Interactive Discussion](#)


Srivastava, R. K., McRae, D., and Odman, M.: An adaptive grid algorithm for air-quality modeling, *J. Comput. Phys.*, 165, 437–472, 2000. 4340

Staniforth, A., Côté, J., and Pudykiewicz, J.: Comments on “Swolarkiewicz’s Deformational Flow”, *Mon. Weather Rev.*, 115, 894–900, 1987. 4347, 4351, 4352

5 Sweby, P. K.: High resolution schemes using flux limiters for hyperbolic conservation laws, *SIAM J. Numer. Anal.*, 21, 995–1011, 1984. 4343

Walcek, C. J. and Aleksic, N. M.: A simple but accurate mass conservative, peak-preserving, mixing ratio bounded advection algorithm with FORTRAN code, *Atmos. Environ.*, 32, 3863–3880, 1998. 4339, 4347, 4351, 4352

10 Wang, Y.: An explicit simulation of Tropical cyclones with a triply nested movable mesh primitive equation model: TCM3. Part I: Model description and control experiment, *Mon. Weather Rev.*, 129, 1370–1394, 2001. 4339

Waterson, N. P. and Deconinck, H.: Design principles for bounded higher-order convection schemes—a unified approach, *J. Comput. Phys.*, 224, 182–207, 2007. 4343

15 Weller, H., Ringler, T., Piggott, M., and Wood, N.: Challenges facing adaptive mesh modeling of the atmosphere and ocean, *B. Am. Meteorol. Soc.*, 91, 105–108, 2010. 4338

Wilson, C.: Modelling multiple-material flows on adaptive unstructured meshes, PhD thesis, Imperial College London, 2009. 4343

20 Zhang, D.-L., Chang, H.-R., Seaman, N. L., Warner, T. T., and Fritsch, J. M.: A two-way interactive nesting procedure with variable terrain resolution, *Mon. Weather Rev.*, 114, 1330–1339, 1986. 4339

A new multiscale air pollutant transport model using anisotropic adaptive mesh methods

J. Zheng et al.

Title Page

Abstract

Introduction

Conclusions

References

Tables

Figures

◀

▶

◀

▶

Back

Close

Full Screen / Esc

Printer-friendly Version

Interactive Discussion

Table 1. Basic configuration for FEM_Adapt_L and FEM_Fix_L schemes (where FEM represents CV or DG; the maximum mesh size is set to be 0.2).

Mesh schemes (L)		1	2	4	8	128
Minimum mesh size (h)		0.01	0.005	0.0025	0.00125	7.8125×10^{-6}
The maximum number of nodes	FEM_Adapt_L	3500	7500	15 000	25 000	45 000
The number of nodes	FEM_Fix_L	10 201	40 401	160 801	641 601	163 865 601

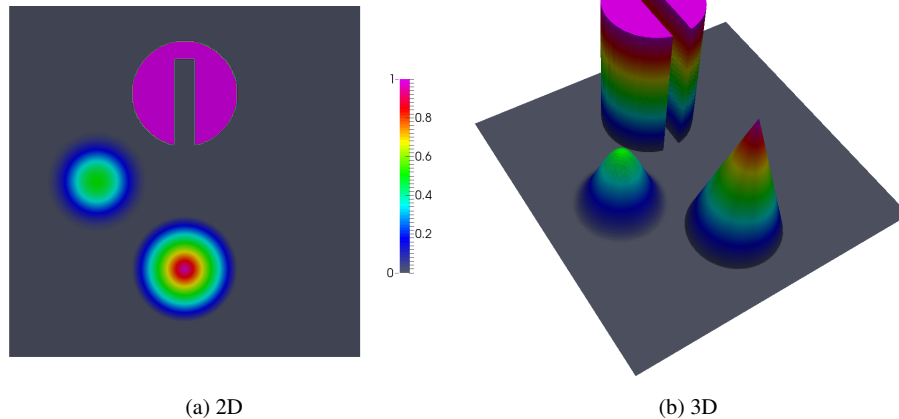


Figure 1. Initial distribution/exact solution at $t = 2\pi$ in 2-D and 3-D view.

A new multiscale air pollutant transport model using anisotropic adaptive mesh methods

J. Zheng et al.

Title Page	
Abstract	Introduction
Conclusions	References
Tables	Figures
◀	▶
◀	▶
Back	Close
Full Screen / Esc	
Printer-friendly Version	
Interactive Discussion	



A new multiscale air pollutant transport model using anisotropic adaptive mesh methods

J. Zheng et al.

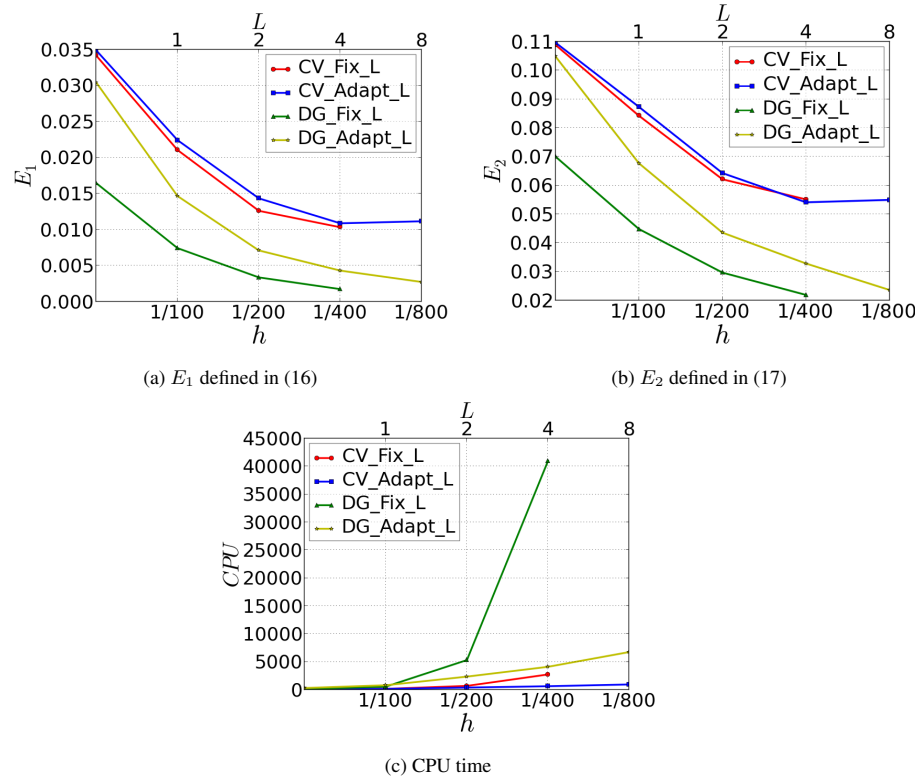


Figure 2. Case one – solid body revolution: the errors in the c field solutions and the CPU time (as a function of the mesh size h) required for one revolution, where h is the mesh size for FEM_Fix_L schemes while the minimum mesh size for FEM_Adapt_L schemes, using the same $\Delta t = 0.01$.

[Title Page](#)

[Abstract](#)

[Introduction](#)

[Conclusions](#)

[References](#)

[Tables](#)

[Figures](#)

[⏪](#)

[⏩](#)

[◀](#)

[▶](#)

[Back](#)

[Close](#)

[Full Screen / Esc](#)

[Printer-friendly Version](#)

[Interactive Discussion](#)



A new multiscale air pollutant transport model using anisotropic adaptive mesh methods

J. Zheng et al.

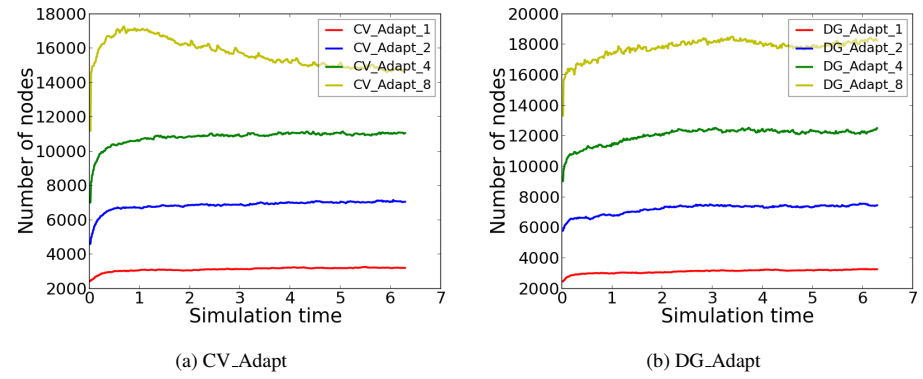


Figure 3. Case one – solid body revolution: the evolution of number of nodes for **(a)** CV_Adapt, **(b)** DG_Adapt.

Title Page

Abstract

Introduction

Conclusions

References

Tables

Figures

⏪

⏩

◀

▶

Back

Close

Full Screen / Esc

Printer-friendly Version

Interactive Discussion



A new multiscale air pollutant transport model using anisotropic adaptive mesh methods

J. Zheng et al.

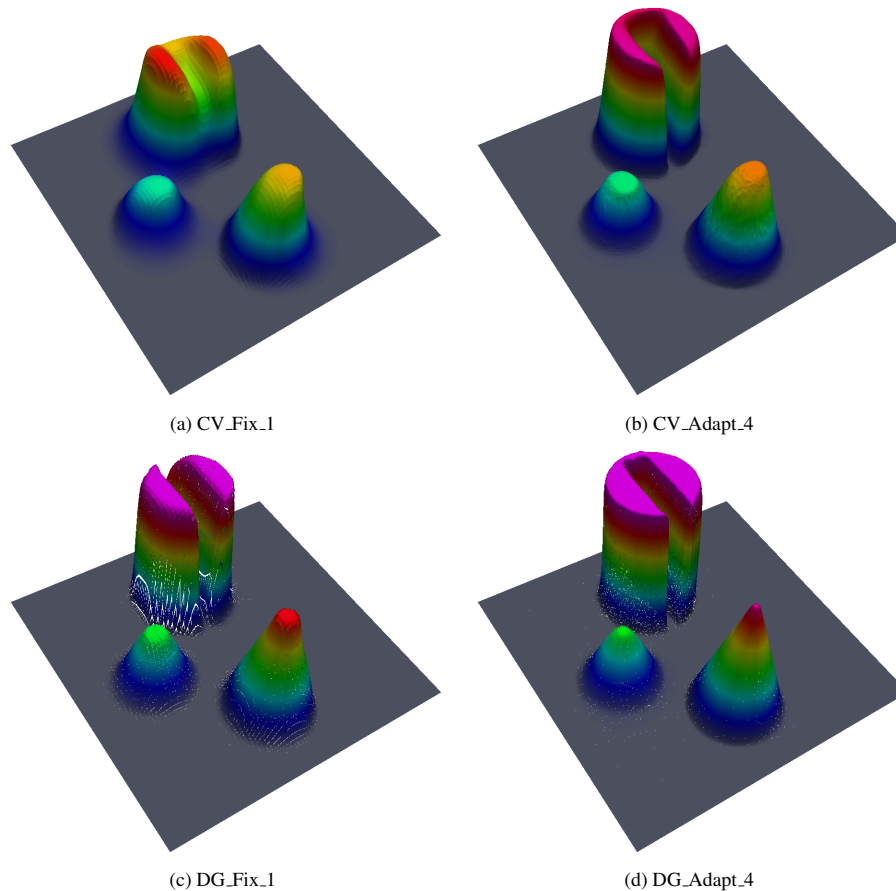


Figure 4. Case one – solid body revolution: the results from the fixed and adaptive mesh schemes using almost the same nodes number N , where $N = 10\,201$ for FEM_Fix_1 scheme while $N \approx 11\,500$ for FEM_Adapt_4 scheme, at $t = 2\pi$.

[Title Page](#)
[Abstract](#)
[Introduction](#)
[Conclusions](#)
[References](#)
[Tables](#)
[Figures](#)
[I ◀](#)
[▶ I](#)
[◀](#)
[▶](#)
[Back](#)
[Close](#)
[Full Screen / Esc](#)
[Printer-friendly Version](#)
[Interactive Discussion](#)

A new multiscale air pollutant transport model using anisotropic adaptive mesh methods

J. Zheng et al.

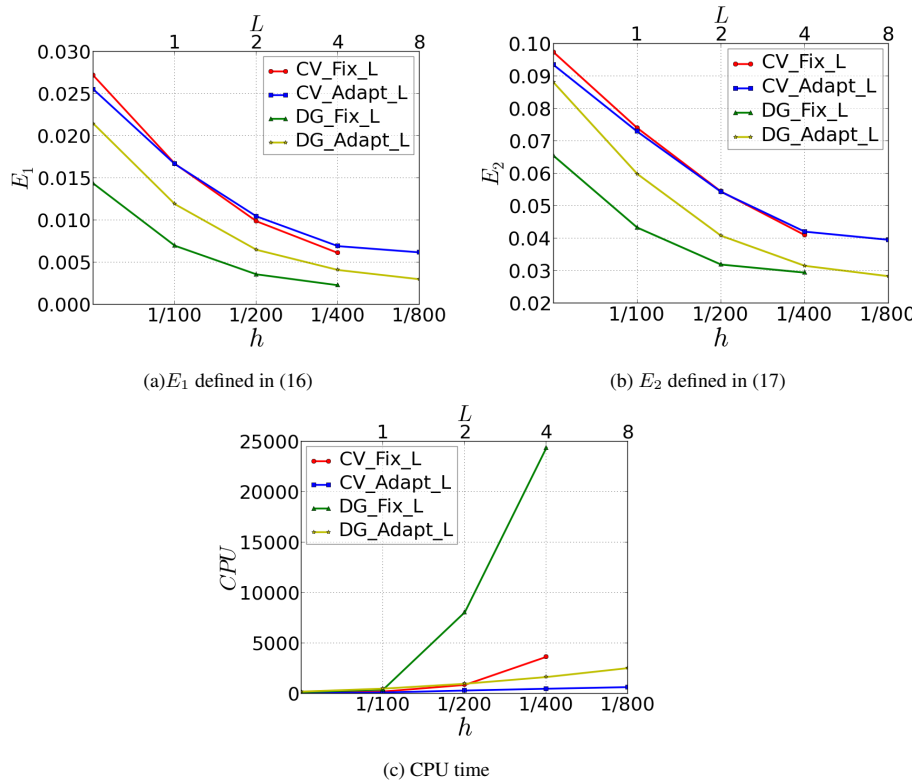


Figure 5. Case two – swirling flow: the errors in the c field solutions and the CPU time (as a function of the mesh size h) required for one revolution, where h is the mesh size for FEM_Fix_L schemes while the minimum mesh size for FEM_Adapt_L schemes, using the same $\Delta t = 0.0025$.

Title Page

Abstract Introduction

Conclusions References

Tables Figures

⏪ ⏩

◀ ▶

Back Close

Full Screen / Esc

Printer-friendly Version

Interactive Discussion



A new multiscale air pollutant transport model using anisotropic adaptive mesh methods

J. Zheng et al.

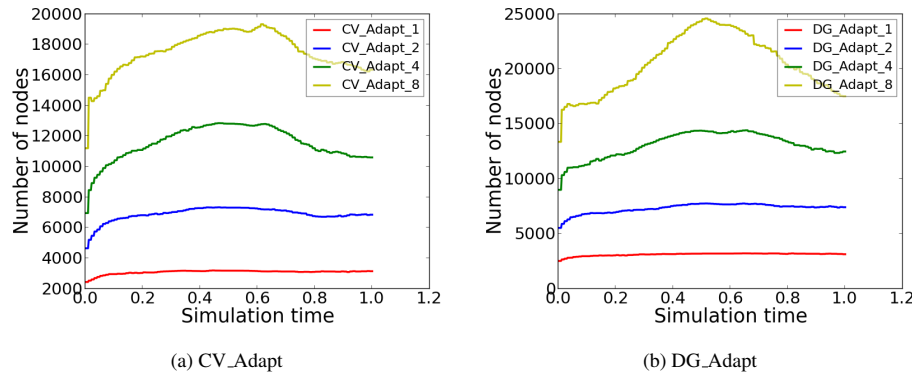


Figure 6. Case two – swirling flow: the evolution of number of nodes for **(a)** CV_Adapt, **(b)** DG_Adapt.

Title Page

Abstract	Introduction
Conclusions	References
Tables	Figures

⏪
⏩

◀
▶

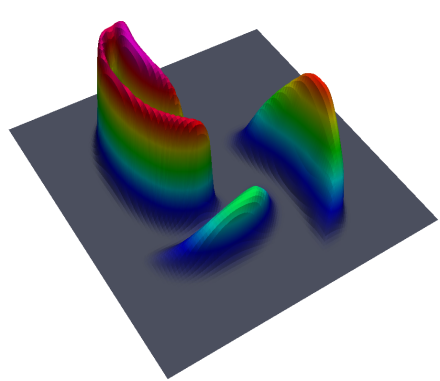
Back	Close
------	-------

Full Screen / Esc

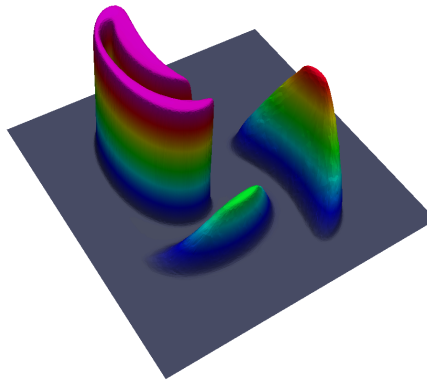
Printer-friendly Version

Interactive Discussion

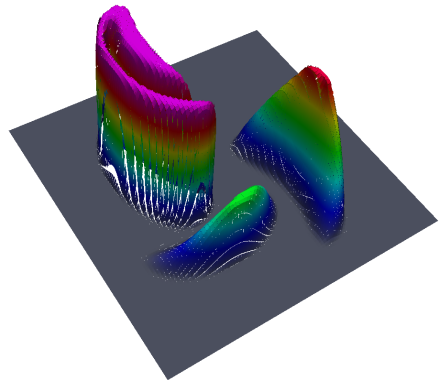




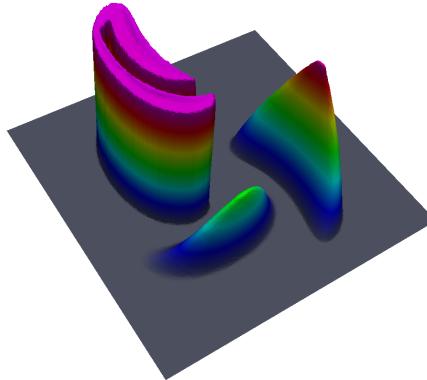
(a) CV_Fix_1



(b) CV_Adapt_4



(c) DG_Fix_1



(d) DG_Adapt_4

Figure 7. Case two – swirling flow: the results from the fixed and adaptive mesh schemes using almost the same nodes N , where $N = 10\,201$ for FEM_Fix_1 scheme while $N \approx 12\,000$ for FEM_Adapt_4 scheme, at $t = T/2 (= 0.5)$.

A new multiscale air pollutant transport model using anisotropic adaptive mesh methods

J. Zheng et al.

Title Page

Abstract

Introduction

Conclusions

References

Tables

Figures

⏪

⏩

◀

▶

Back

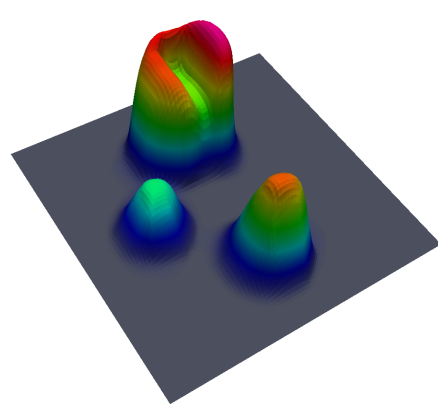
Close

Full Screen / Esc

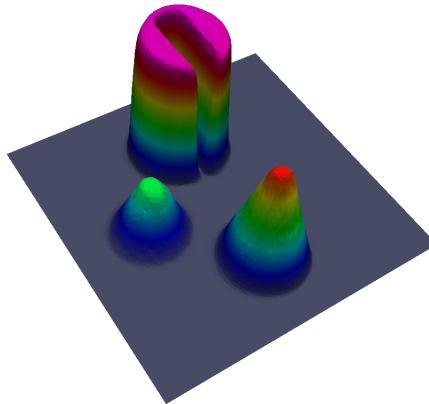
Printer-friendly Version

Interactive Discussion

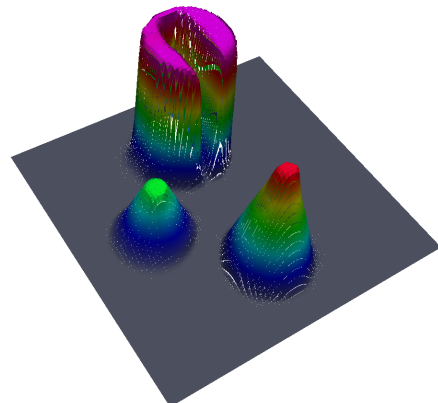




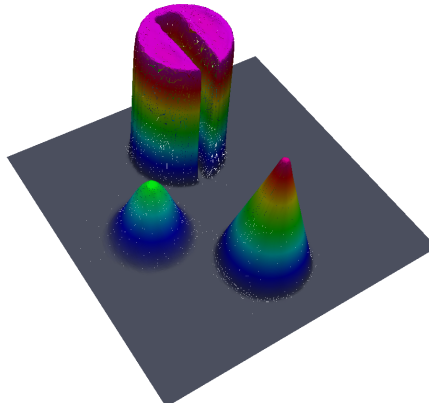
(a) CV_Fix_1



(b) CV_Adapt_4



(c) DG_Fix_1



(d) DG_Adapt_4

Figure 8. Case two – swirling flow: the results from the fixed and adaptive mesh schemes using almost the same nodes number N , where $N = 10\,201$ for FEM_Fix_1 scheme while $N \approx 12\,000$ for FEM_Adapt_4 scheme, at $t = T (= 1)$.

A new multiscale air pollutant transport model using anisotropic adaptive mesh methods

J. Zheng et al.

Title Page

Abstract

Introduction

Conclusions

References

Tables

Figures

⏪

⏩

◀

▶

Back

Close

Full Screen / Esc

Printer-friendly Version

Interactive Discussion



A new multiscale air pollutant transport model using anisotropic adaptive mesh methods

J. Zheng et al.

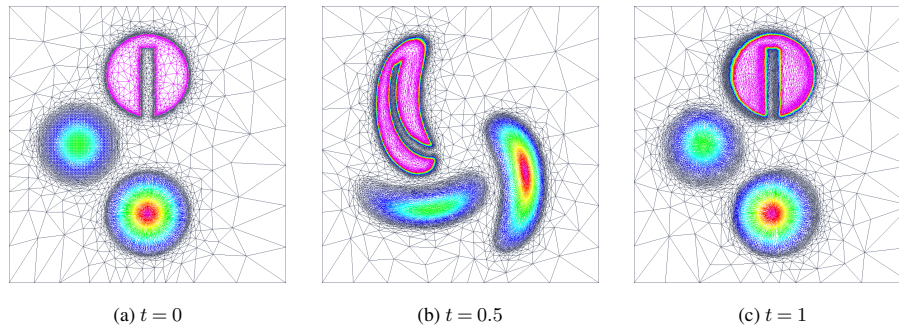


Figure 9. Case two – swirling flow: the evolution of the adaptive mesh colored with tracer value c , where DG_Adapt_4 scheme is used.

[Title Page](#)[Abstract](#)[Introduction](#)[Conclusions](#)[References](#)[Tables](#)[Figures](#)[⏪](#)[⏩](#)[◀](#)[▶](#)[Back](#)[Close](#)[Full Screen / Esc](#)[Printer-friendly Version](#)[Interactive Discussion](#)

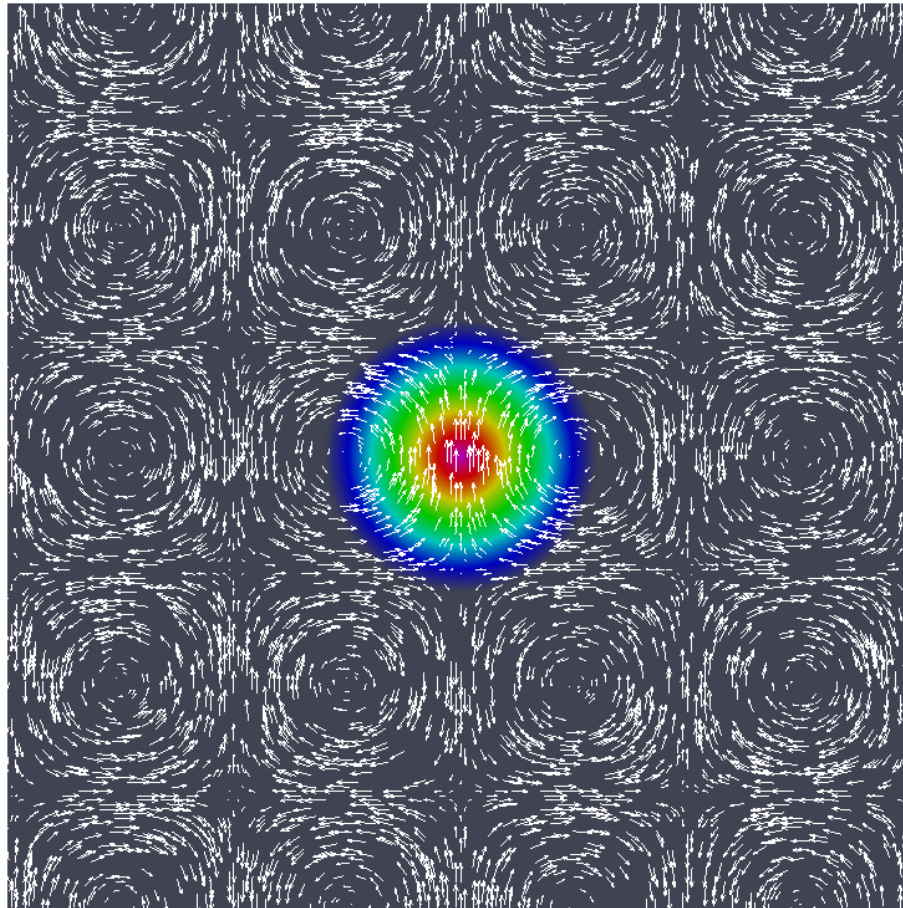


Figure 10. Case three – swirling deformation: initial distribution and velocity field.

A new multiscale air pollutant transport model using anisotropic adaptive mesh methods

J. Zheng et al.

Title Page

Abstract

Introduction

Conclusions

References

Tables

Figures

◀

▶

◀

▶

Back

Close

Full Screen / Esc

Printer-friendly Version

Interactive Discussion

A new multiscale air pollutant transport model using anisotropic adaptive mesh methods

J. Zheng et al.

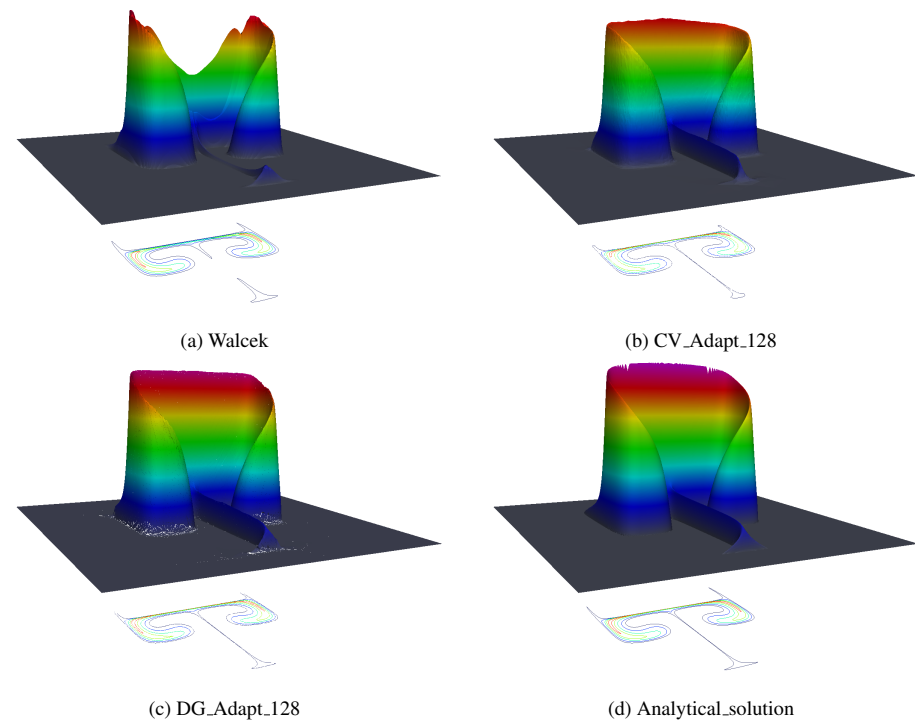


Figure 11. Case three – swirling deformation: comparison of the analytical solution with the results from different schemes using almost the same number of nodes $N \approx 40\,000$, at $t = 3T/20$, where $T = 2.6376$.

Title Page	
Abstract	Introduction
Conclusions	References
Tables	Figures
◀	▶
◀	▶
Back	Close
Full Screen / Esc	
Printer-friendly Version	
Interactive Discussion	



A new multiscale air pollutant transport model using anisotropic adaptive mesh methods

J. Zheng et al.

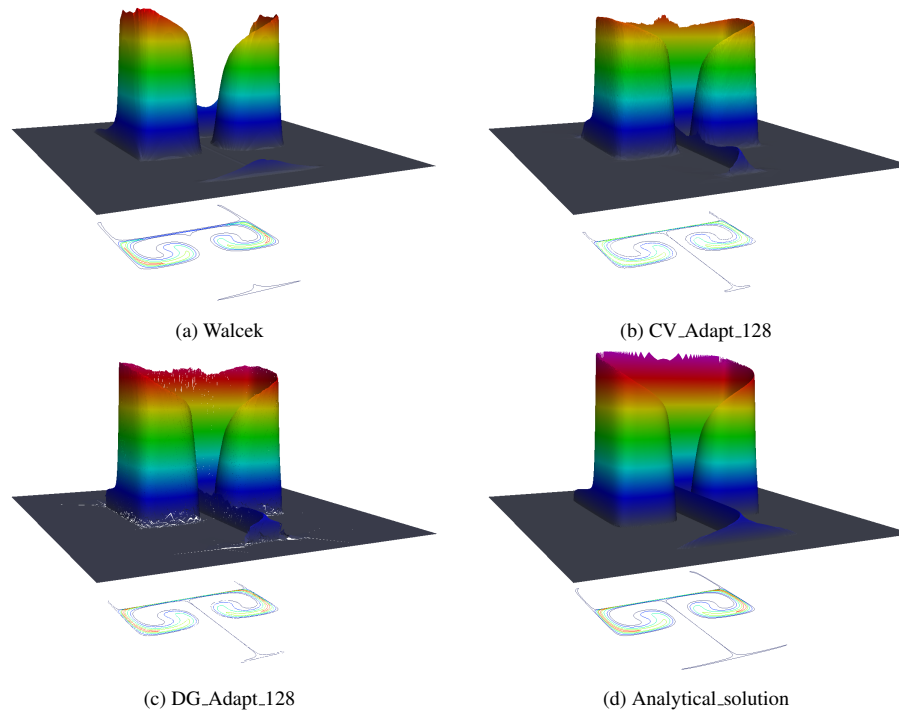


Figure 12. Case three – swirling deformation: comparison of the analytical solution with the results from different schemes using almost the same number of nodes $N \approx 40\,000$, $t = T/5$, where $T = 2.6376$.

[Title Page](#)[Abstract](#)[Introduction](#)[Conclusions](#)[References](#)[Tables](#)[Figures](#)[⏪](#)[⏩](#)[◀](#)[▶](#)[Back](#)[Close](#)[Full Screen / Esc](#)[Printer-friendly Version](#)[Interactive Discussion](#)

A new multiscale air pollutant transport model using anisotropic adaptive mesh methods

J. Zheng et al.

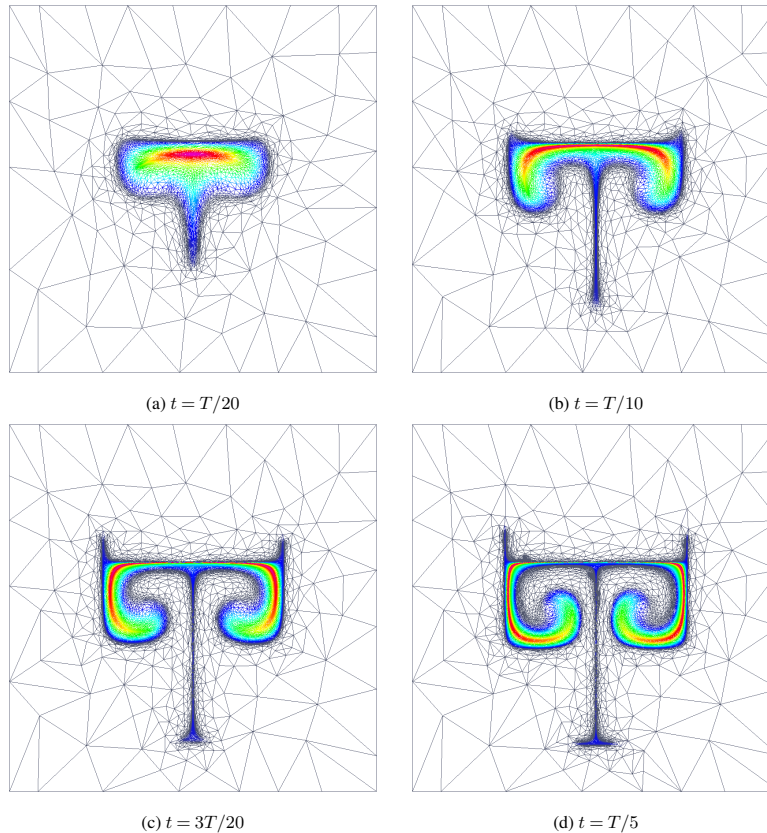


Figure 13. Case three – swirling deformation: the evolution of the adaptive mesh colored with tracer value c , where DG_Adapt_128 scheme is used.

Title Page

Abstract

Introduction

Conclusions

References

Tables

Figures

◀

▶

◀

▶

Back

Close

Full Screen / Esc

Printer-friendly Version

Interactive Discussion

A new multiscale air pollutant transport model using anisotropic adaptive mesh methods

J. Zheng et al.

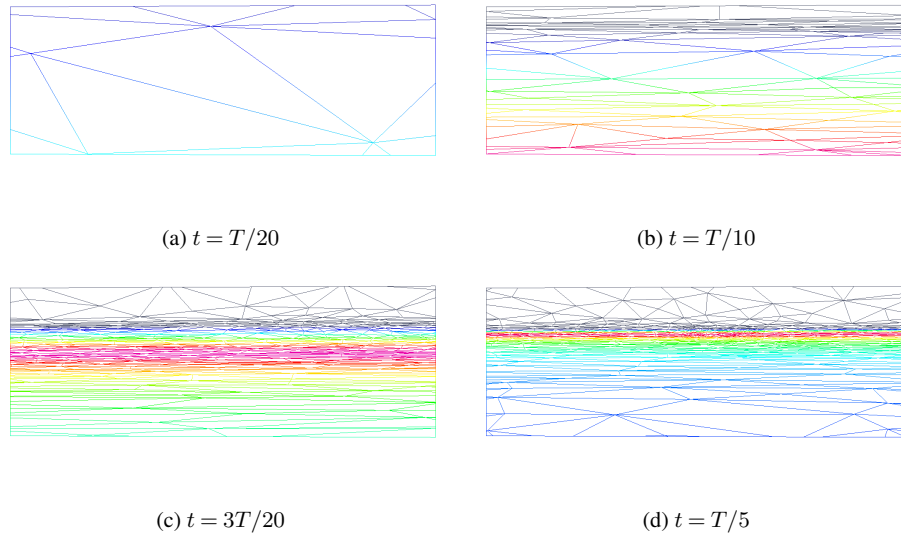


Figure 14. Case three – swirling deformation: the evolution of the adaptive mesh colored with tracer value c , in the subdomain $[0.49, 0.51] \times [0.62, 0.627]$, using DG_Adapt_128 scheme.

Title Page

Abstract

Introduction

Conclusions

References

Tables

Figures

◀

▶

◀

▶

Back

Close

Full Screen / Esc

Printer-friendly Version

Interactive Discussion



GMDD

8, 4337–4374, 2015

A new multiscale air pollutant transport model using anisotropic adaptive mesh methods

J. Zheng et al.

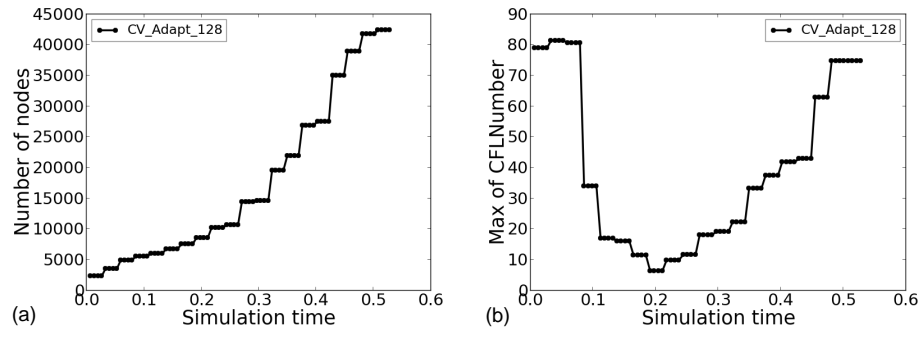


Figure 15. Case three – swirling deformation: the evolution of **(a)** number of nodes, **(b)** max local CFL number for CV_Adapt_128 schemes.

Title Page	
Abstract	Introduction
Conclusions	References
Tables	Figures
◀	▶
◀	▶
Back	Close
Full Screen / Esc	
Printer-friendly Version	
Interactive Discussion	

